RADIO SCIENCE Journal of Research NBS/USNC-URSI
Vol. 69D, No. 5, May 1965

A Systematic Study of the Radiation Patterns of a Dipole in a Magnetoplasma Based on a Classification of the Associated Dispersion Surfaces

R. Mittra and G. L. Duff

Antenna Laboratory, University of Illinois, Urbana, Ill.

(Received October 1, 1964; revised December 4, 1964)

This study commences by demonstrating the important role played by the dispersion surfaces in the determination of the far fields of an infinitesimal dipole in a lossless, cold magneto-ionic medium. The dispersion surfaces are then classified, according to their shapes, for different ranges of the plasma parameters. A comprehensive group of radiation patterns is then given including far fields for each of the fourteen classified ranges of the plasma parameters.

1. Introduction

In recent years considerable attention has been directed towards the study of radiation from sources in anisotropic media of an infinite homogeneous nature. It is of great interest to study the case of a cold lossless medium for different combinations of electron density and applied steady magnetic field. The Appleton-Hartree equation constitutes the mathematical description of the "plasma" that is often used in this analysis. This problem has been studied extensively [Bunkin, 1957; Kuehl, 1960; Arbel, 1960; Arbel and Felsen, 1963; Kogelnik and Motz, 1963; Wait, 1964]. Of more specific interest are the far fields of an infinitesimal dipole. Analytic expressions for the asymptotic fields have been available for some time in the literature cited above but no extensive numerical calculations have been made for the far field patterns of a short dipole. It should be noted that Arbel and Felsen [1963] have numerically computed the "pattern factors" of the individual ray contributions for the longitudinal electric dipole. The "pattern factors" were calculated for 8 different sets of the parameters X and Y in the general vicinity of $X=1$, $Y=1$ and the ordinary and extraordinary "patterns" are shown, but not the total field patterns.

The purpose of this study is to briefly summarize Kuehl's method of calculation, to demonstrate the important role the dispersion surfaces play in the calculation of the far fields and to classify these various types of dispersion surfaces according to specific ranges of the plasma parameters. Explicitly, these parameters are the electron density, applied steady magnetic field and frequency, which may be conveniently represented in terms of the dimensionless parameters X and Y, to be defined later. The study embraces infinite, anisotropic, homogeneous media and treats only the lossless case of a cold plasma. The paper includes a brief description of numerical calculation techniques, and the study concludes with the presentation of the far field patterns of an infinitesimal, longitudinal electric dipole calculated for several different combinations of the plasma parameters. The far field patterns are shown in spherical coordinates for the ordinary and extraordinary wave contributions, as well as the total field patterns.

2. Theoretical Considerations

Maxwell's equations in an anisotropic homogeneous medium with a relative permittivity dyadic $\overline{\overline{K}}$ and free space permeability μ_0 are

$$\nabla \times \overline{H} = j\omega\epsilon_0 \overline{\overline{K}}\,\overline{E} + \overline{J} \tag{1}$$

$$\nabla \times \overline{E} = -j\omega\mu_0 \overline{H} \tag{2}$$

where $\overline{E}$ and $\overline{H}$ are electric and magnetic field vectors, $\overline{J}$ is the current density, and ω is the angular frequency. A harmonic time dependence of $e^{j\omega t}$ is assumed.

In a plasma with a $\hat{z}$-directed steady magnetic field, the relative permittivity dyadic $\overline{\overline{K}}$ is of the form

$$\overline{\overline{K}} = \hat{x}\hat{x}K' + j\hat{x}\hat{y}K'' - j\hat{y}\hat{x}K'' + \hat{y}\hat{y}K' + \hat{z}\hat{z}K_0 \tag{3}$$

where

$$K_0 = 1 - \frac{X}{U},\quad K' = 1 - \frac{XU}{U^2 - Y^2},\quad K'' = -\frac{XY}{Y^2 - U^2}$$

$$X = \frac{\omega_N^2}{\omega^2}$$

$$Y = \frac{\omega_H}{\omega},\quad \omega_N^2 = \frac{Ne^2}{m\epsilon_0}\omega_H = \frac{eB_0}{m} \text{ (a positive number).}$$

$$U = 1 - jZ = 1 - j\frac{\nu}{\omega} \text{ (ν = collision frequency).}$$

N = electron density.

B_0 = d-c magnetic flux density.

e = magnitude of electron charge.

m = electron mass.

$k_0 = 2\pi/\lambda_0$ = free space wave number.

λ_0 = free space wavelength.

Taking curl of (2) and using (1), obtain

$$\nabla \times \nabla \times \overline{E} - \omega^2\mu_0\epsilon_0 \overline{\overline{K}}\,\overline{E} = -j\omega\mu_0 \overline{J}. \tag{4}$$

A general solution of (4) may be expressed as

$$\overline{E}(\overline{r}) = \int_v \overline{\overline{\Gamma}}(\overline{r}, \overline{r}') \cdot \overline{J}(\overline{r}')dv' \tag{5}$$

where $\overline{\overline{\Gamma}}(\overline{r}, \overline{r}')$ is the dyadic Green's function, the integration being performed over the volume v containing the source currents. Note that

$$\overline{J}(\overline{r}) = \int_v \overline{\overline{U}}\,\overline{J}(\overline{r}')\delta(\overline{r} - \overline{r}')dv' \tag{6}$$

where $\overline{\overline{U}}$ is the unit dyadic, and $\delta(\bar{r})$ is the three-dimensional Dirac delta function. Substituting (5) and (6) into (4) and using some well-known vector identities we obtain the following equation satisfied by the dyadic Green's function:

$$(-\nabla^2\overline{\overline{U}}+\nabla\nabla-\omega^2\mu_0\epsilon_0\overline{\overline{K}})\overline{\overline{\Gamma}}(\bar{r})=-j\omega\mu_0\overline{\overline{U}}\delta(\bar{r}). \tag{7}$$

Now define the three-dimensional Fourier transform pair:

$$\overline{\overline{f}}(\bar{\kappa})=\int_{-\infty}^{\infty}\overline{\overline{f}}(\bar{r})e^{j\bar{\kappa}\cdot\bar{r}}d\bar{r},\quad \overline{\overline{f}}(\bar{r})=\frac{1}{(2\pi)^3}\int_{-\infty}^{\infty}\overline{\overline{f}}(\bar{\kappa})e^{-j\bar{\kappa}\cdot\bar{r}}d\bar{\kappa}.$$

Transforming (7) and letting

$$\overline{\overline{M}}(\bar{\kappa})=\bar{\kappa}\cdot\bar{\kappa}\overline{\overline{U}}-\bar{\kappa}\bar{\kappa}-\omega^2\mu_0\epsilon_0\overline{\overline{K}} \tag{8}$$

one obtains

$$\overline{\overline{M}}(\bar{\kappa})\overline{\overline{\Gamma}}(\bar{\kappa})=-j\omega\mu_0\overline{\overline{U}}.$$

Premultiplying by $\overline{\overline{M}}^{-1}$ and taking the inverse Fourier transform one obtains:

$$\overline{\overline{\Gamma}}(\bar{r})=-\frac{j\omega\mu_0}{8\pi^3}\int_{-\infty}^{\infty}\overline{\overline{M}}^{-1}e^{-j\bar{\kappa}\cdot\bar{r}}d\bar{\kappa} \tag{9}$$

where $M^{-1}=\dfrac{\overline{\overline{P}}}{|\overline{\overline{M}}|}$.

Removing $\overline{\overline{P}}$ outside the integral in its *operator* form, $\overline{\overline{D}}$, we have

$$\overline{\overline{\Gamma}}(\bar{r})=\frac{j\omega\mu_0}{8\pi^3}\overline{\overline{D}}\int_{-\infty}^{\infty}\frac{1}{|\overline{\overline{M}}|}e^{-j\bar{\kappa}\cdot\bar{r}}d\bar{\kappa}. \tag{10}$$

$$\text{Now } |\overline{\overline{M}}|=-\omega^2\mu_0\epsilon_0K_0(\kappa_z^2-s_z^2)(\kappa_z^2-t_z^2) \tag{11}$$

where s_z and t_z are the roots of $|\overline{\overline{M}}|=0$ [Allis et al., 1963]. Next consider the asymptotic evaluation of the integral appearing in (10). Let

$$I(\bar{r})=\int_{-\infty}^{\infty}\int_{-\infty}^{\infty}\int_{-\infty}^{\infty}\frac{e^{-j\bar{\kappa}\cdot\bar{r}}}{(\kappa_z^2-s_z^2)(\kappa_z^2-t_z^2)}d\kappa_x d\kappa_y d\kappa_z. \tag{12}$$

Integrate the above equation over κ_z using the calculus of residues and transform the x, y, z system to a r, θ, ϕ spherical coordinate system. Also the transform variables κ_x and κ_y can be transformed into a polar coordinate system, ρ, β. After integrating over β the remaining integral can be evaluated using the saddle point method for large k_0r, the result being that asymptotically

$$I(\bar{r})=\frac{1}{k_0r}\sum_{m=1}^{2}\sum_{n}(-1)^mA_{mn}(\theta)e^{-j\chi_{mn}(\theta)k_0r} \tag{13}$$

where $A_{mn}(\theta) = -\left(\dfrac{2\pi^2 j \cos\theta}{k_0^3 \sqrt{\sin\theta}\cos(\psi_{mn}-\theta)\cos\psi_{mn}}\right)$

$$\times \sqrt{\frac{n_m \operatorname{Sin}\psi_{mn}}{[(K'-K_0)^2 n_{mn}^4 \operatorname{Sin}^4\psi_{mn} - 4K_0K'^2(n_{mn}^2 \operatorname{Sin}^2\psi_{mn} - K_0)]\,[(n''_{mn}-n_{mn})\operatorname{Cos}(\psi_{mn}-\theta) - 2n'_{mn}\operatorname{Sin}(\psi_{mn}-\theta)]}} \tag{14a}$$

and

$$\chi_{mn}(\theta) = n_{mn}(\psi_{mn})\operatorname{Cos}(\psi_{mn}-\theta). \tag{14b}$$

Note that if n_m is imaginary, $e^{-jx_{mn}k_0 r}$ decays exponentially and there will be no far field; n'_{mn} and n''_{mn} denote the first and second derivative of n_m respectively, evaluated at ψ_{mn}. Here

$$n_m^2(\psi) = \frac{[K'(K'-K_0)-K'^2]\operatorname{Sin}^2\psi + 2K'K_0 \pm \sqrt{[K'(K'-K_0)-K'^2]^2 \operatorname{Sin}^4\psi + 4K_0^2K''^2\cos^2(\psi)}}{2(K'\operatorname{Sin}^2\psi + K_0\operatorname{Cos}^2\psi)}, \tag{15}$$

$n_m(\psi)$, $m=1$, 2 (ordinary, extraordinary), are the two dispersion curves and the saddle point condition is

$$\frac{d}{d\psi}[n_m(\psi_m)\operatorname{Cos}(\psi_m-\theta)] = 0,\ m=1, \text{ and } 2, \text{ i.e., } \frac{d}{d\psi}(n_m) = n_m \tan(\psi-\theta). \tag{16}$$

Equation (16) may have more than 1 solution, and these solutions can be identified by ψ_{mn} where n may be 1, 2, or 3, depending on the shape of the n_m curves. The details of this evaluation are to be found in Kuehl [1960]. The dyadic operator $\bar{\bar{D}}$ must now be evaluated in the coordinate system (r, θ, ϕ), to finally yield $\bar{\bar{\Gamma}}(\bar{r})$, the Green's dyadic, which can be regarded as a 3×3 matrix. To calculate the far fields of a $\hat{z}$-directed infinitesimal dipole only three of these 9 components need be calculated. They are

$$\Gamma_{xz} = G\sum_{m=1}^{2}\sum_{n}\left((-1)^m n_{mn}^2 \operatorname{Sin}\psi_{mn}\operatorname{Cos}\psi_{mn}[(n_{mn}^2-K')\operatorname{Cos}\phi - jK''\operatorname{Sin}\phi]F_{mn}\right) \tag{17}$$

$$\Gamma_{yz} = G\sum_{m=1}^{2}\sum_{n}\left((-1)^m n_{mn}^2 \operatorname{Sin}\psi_{mn}\operatorname{Cos}\psi_{mn}[(n_{mn}^2-K')\operatorname{Sin}\phi + jK''\operatorname{Cos}\phi]F_{mn}\right) \tag{18}$$

$$\Gamma_{zz} = G\sum_{m=1}^{2}\sum_{n}\left((-1)^m[(n_{mn}^2-K')(n_{mn}^2\operatorname{Cos}^2\psi_{mn}-K') - K''^2]F_{mn}\right) \tag{19}$$

where

$$G = \frac{j\omega\mu_0 k_0^3}{8\pi^3 r} \text{ and } F_{mn} = A_{mn}(\theta)\, e^{-jx_{mn}(\theta)k_0 r}. \tag{20}$$

The infinitesimally small dipole of dipole moment $\bar{p}$ located at the origin yields an electric field given by

$$\bar{E}(\bar{r}) = j\omega\bar{\bar{\Gamma}}(\bar{r})\bar{p}. \tag{21}$$

This equation may be employed to calculate the far field patterns after inserting the asymptotic form of $\bar{\bar{\Gamma}}(\bar{r})$ in (21).

3. Refractive Index Surfaces

As was demonstrated in the previous section the refractive index surfaces, $n_m(\psi)$, $m=1$, 2, play an important role in the determination of the far fields of a source in a plasma. It is neces-

sary to have a description of the refractive index surfaces for each mode of propagation. The shape of these surfaces is a function of the dimensionless parameters X and Y which are used to describe the lossless ($Z=0$) medium. These surfaces are surfaces of revolution about an axis parallel to the direction of the imposed steady magnetic field. Thus two-dimensional plots of the curves, which are cross sections of the surfaces in an axial plane, serve to describe the complex refractive index surfaces. Another form of (15) in terms of X and Y is

$$n_m^2(\theta)=1-X\left[1-\frac{\frac{1}{2}Y^2\sin^2\theta}{1-X}\pm\left\{\left(\frac{\frac{1}{2}Y^2\sin^2\theta}{1-X}\right)^2+Y^2\cos^2\theta\right\}^{1/2}\right]^{-1}. \tag{22}$$

These are the *curves* which describe the above *surfaces* for a lossless anisotropic cold plasma. It is common practice [Ratcliffe, 1962] to associate the subscript $m=1$ with the + sign and the nomenclature 'ordinary wave', and $m=2$ with the − sign and the 'extraordinary', in the lossless case. For the lossless case $n_m^2(\psi)$ is always real for all values of ψ. It should also be noted that $n_m(\psi)=n_m(\pi-\psi)$ and $n_m(\psi)=n_m(-\psi)$. Consequently one need only calculate $n_m(\psi)$ for $0\leq\psi\leq\pi/2$, the rest of the curve being obtained from the above relations. From the last section it is seen that the asymptotic far fields on an infinitesimal dipole are expressible in terms of $n_m(\psi)$, and its first and second derivatives evaluated at the saddle points. Deschamps and Kesler [1964] have recently shown that the far fields of a source in a magnetoplasma may be expressed by

$$\bar{F}(r)=\sum_k\frac{-jh}{4\pi r}(\bar{H}_m^{\dagger}\cdot\bar{\mathscr{M}})\bar{F}_k(r) \tag{23}$$

where h is the Gaussian radius of curvature of the refractive index surfaces, $\bar{\mathscr{M}}$ is a single vector representing electric and magnetic source current densities, $\bar{H}_m$ is the magnetic eigenvector and $\bar{F}_k(r)$ is the characteristic (source-free) field vector. The important point to note is that the Gaussian radius of curvature of the refractive index surfaces is a dominating factor in the determination of the far fields [see also Lighthill, 1960].

It is thus desirable to have a general knowledge of the characteristic shapes of the $n_m(\psi)$ curves that will be generated by different combinations of electron density and imposed steady magnetic field.

Clemmow and Mulally [1955], have classified the refractive index curves into eight distinct types, according to certain features of their shapes. These will henceforth be referred to as the characteristic shapes. The regions of the X-Y plane to which these characteristic shapes correspond were given analytically. This classification is extended and clarified somewhat in this study.

The graph of figure 1 shows the division of the X-Y plane into fourteen separate regions (note that X and Y are plotted on logarithmic scales). Each region is numbered according to the kind of characteristic shape of the refractive index surface that exists for those ranges of values of X and Y. The numbers therein refer to the characteristic shapes shown in the lower right hand part of the graph. The numbers are subscripted 0 or E, indicating whether the characteristic shape is associated with the ordinary or extraordinary wave. Only the real parts of the $n_m(\psi)$ curves are shown. The region where the curves are completely imaginary for all ψ has not been numbered (i.e., $X>1+Y$, $Y<1$). There are no far fields generated when the medium parameters (X, Y) are in this region.

It should be noted that characteristic shapes numbered 2, 4, 6, and 8 have points of inflection for some values of ψ, while the remaining 4 curves have not. Furthermore, curves 1, 2, 3, and 4 are associated with both ordinary and extraordinary waves while characteristic shapes numbered 5, 6, 7, and 8 are associated exclusively with extraordinary waves.

761-367 O-65-2

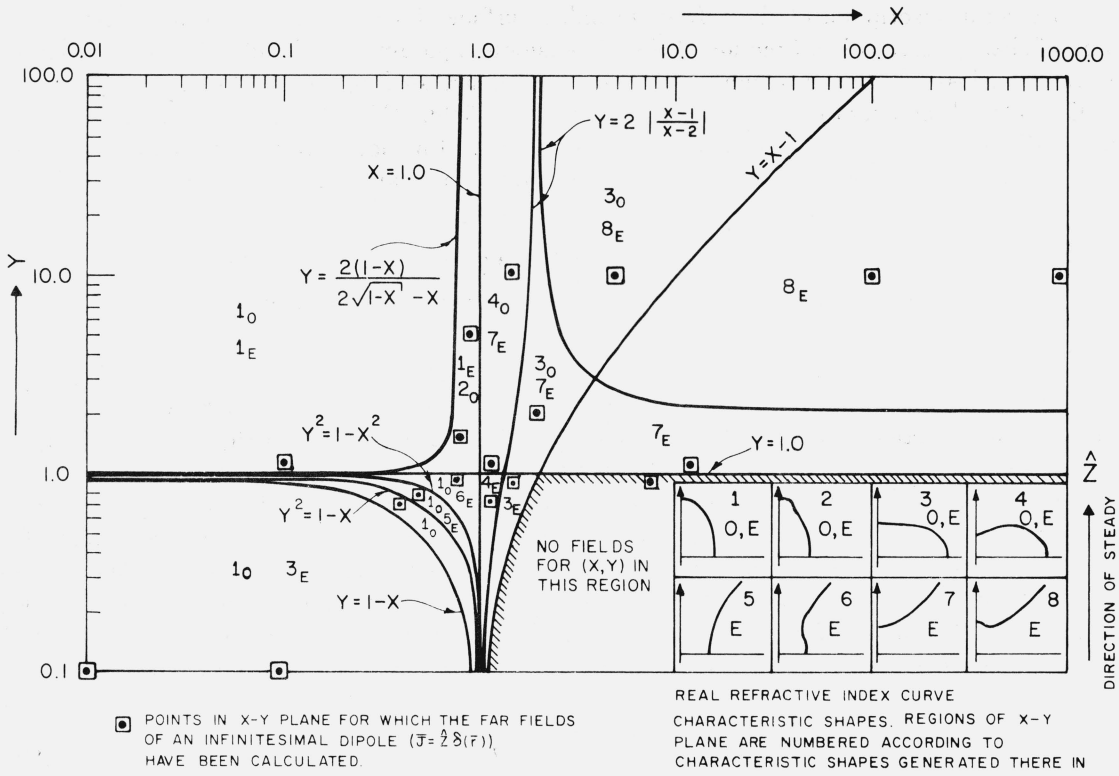

FIGURE 1. *Subdivision of the* X-Y *plane according to the characteristic shapes.*

Some examples of specific values of (X, Y) will now be given:

(a) $X=100$, $Y=10$. This falls within the region marked 8_E. This means that only $n_2(\psi)$ is real and has the characteristic shape shown by curve 8. Thus only an extraordinary wave exists in the far field. Since $n_1(\psi)$ is entirely imaginary for all ψ the ordinary wave does not contribute to the far field.

(b) $X=1.5$, $Y=10$ lies in the region marked 4_0 and 7_E. The ordinary wave is associated with characteristic shape 4 and the extraordinary wave with shape 7.

For a given value of m there may exist more than one saddle point, that is, more than one solution to (16). There can be either one, two, or three saddle points for a given m. The existence of more than one saddle point occurs for some values of θ only for curves containing points of inflection, i.e., those curves numbered 2, 4, 6, and 8. When these curves are encountered there will be a merging of two saddle points at the point of inflection for some value of θ and the single saddle point asymptotic evaluation is no longer valid; one must resort to the double saddle point method of evaluation which involves the Airy integral type of representation [Arbel and Felsen, 1963].

It is to be noted that the present study extends Clemmow and Mulally's [1955] description only in that the ordinary and extraordinary waves are associated with the characteristic shapes of the refractive index curves of each of the 14 regions of the X-Y plane. Furthermore, the diagram of figure 1 facilitates easy identification of the characteristic shape of the dispersion surface for any value of X and Y.

4. Numerical Calculations

The numerical calculation of the far fields of a z-directed dipole, i.e., $\bar{J}=\hat{z}\delta(\bar{r})$, was carried out in four separate stages, for seventeen different sets of (X, Y) as shown on the graph of the X-Y plane embracing all the fourteen regions.

(a) Computation of refractive index curves was done on the University of Illinois IBM 7094 computer using (22). The curves $n_1(\psi)$ and $n_2(\psi)$ were then plotted. The real values of $n_m(\psi)$ indicate propagation while imaginary values indicate cutoff, as seen in (14b).

(b) Computation of the saddle points was accomplished by using a geometrical construction [Mittra and Deschamps, 1963] for the solution of (16) and then iterating to obtain more precise solutions by the Newton-Raphson method. The iterated saddle points were then used as input data to the program for the computation of the far fields.

(c) The saddle point solutions ψ_{mn} for a fixed angle θ were used in (17) through (21) to compute the electric field which was then transformed into spherical components.

(d) In certain cases (where $\psi_{mn}=\theta$) at $\theta=0$ and $\pi/2$ (14a) is an indeterminate form. A modified approach for the calculation of A_{mn} as given by Kuehl [1960] is then employed.

Throughout the calculation $k_0r=100$ was used. It should be pointed out that in general the total fields may be quite dependent on the magnitude of k_0r since it affects the phase between the ordinary and extraordinary waves. This is seen in (13). In some cases the individual ordinary and extraordinary components of the electric field behave in a peculiar fashion, but the vector sum yields total fields of a familiar behavior. This is especially true in the case of a near-isotropic plasma (set No. 3, fig. 2).

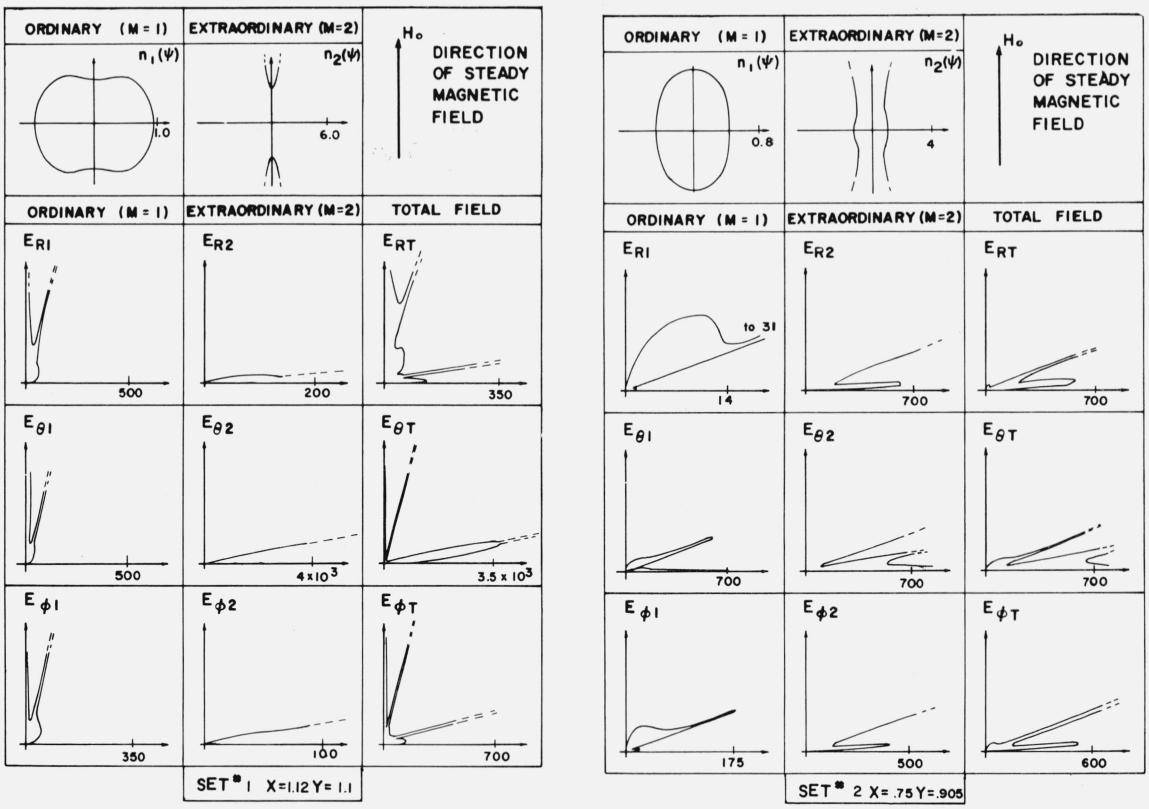

FIGURE 2. *Calculated radiation patterns for different medium parameters.*

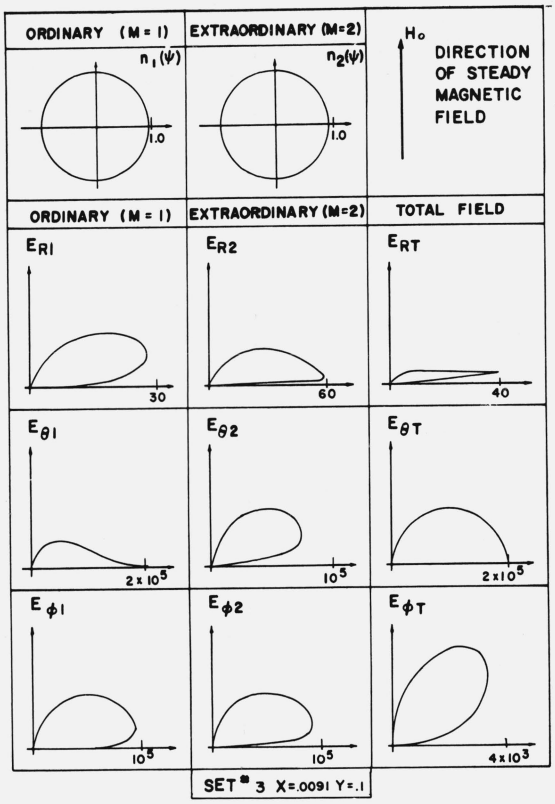

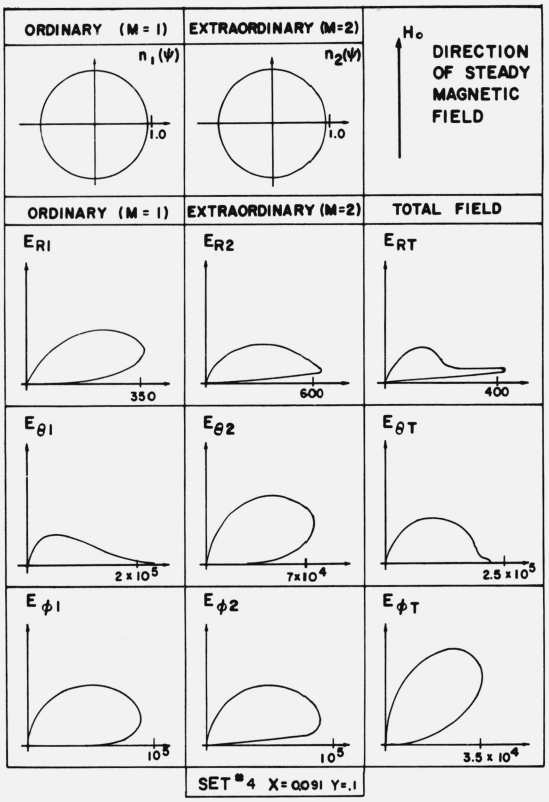

FIGURE 2. *Continued—Calculated radiation patterns for different medium parameters.*

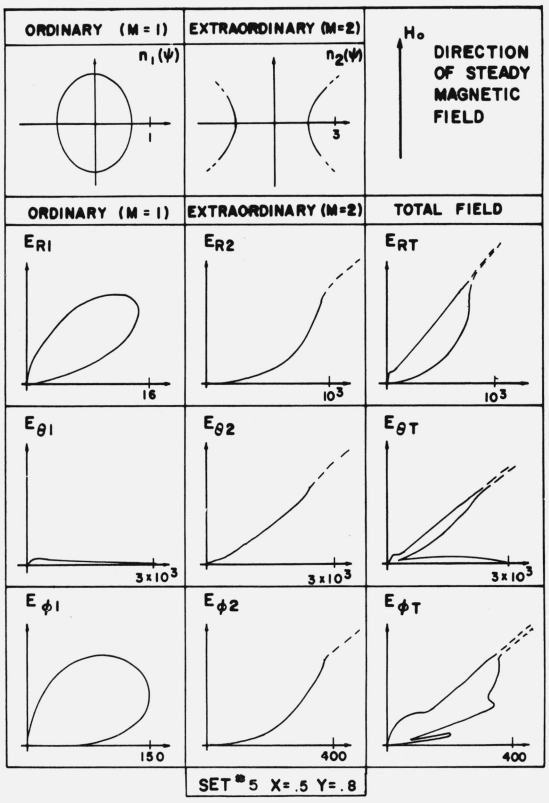

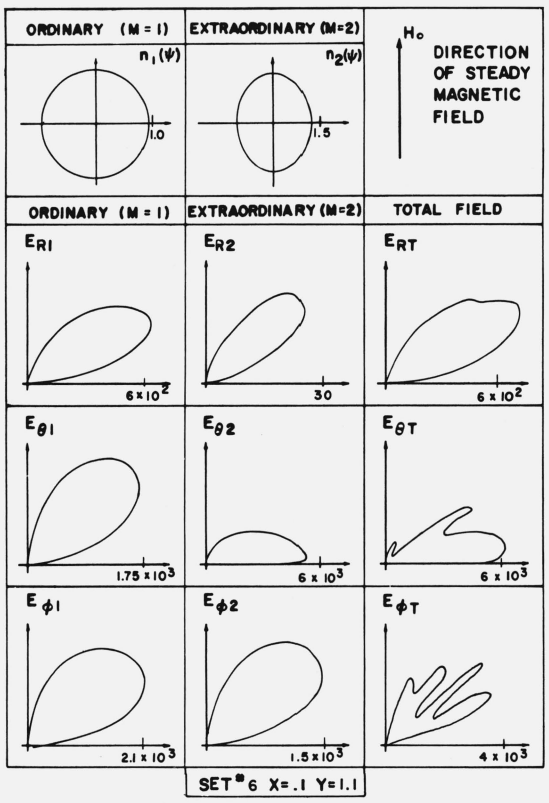

FIGURE 2. *Continued—Calculated radiation patterns for different medium parameters.*

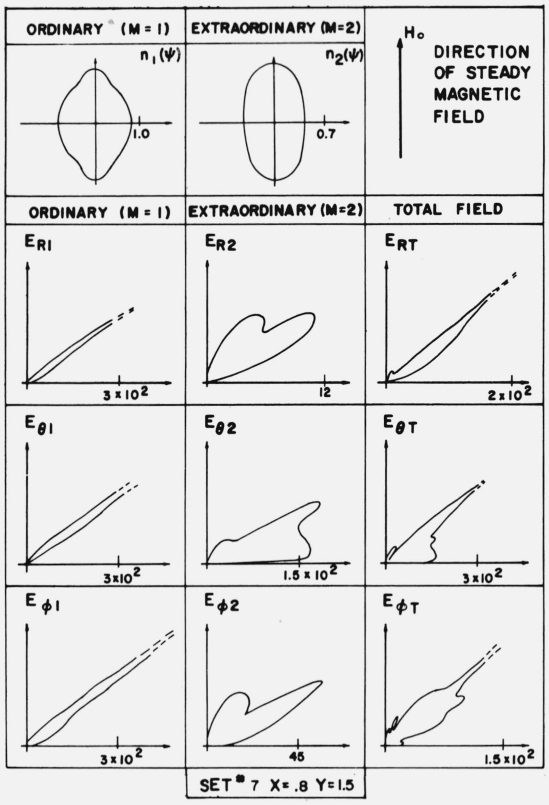

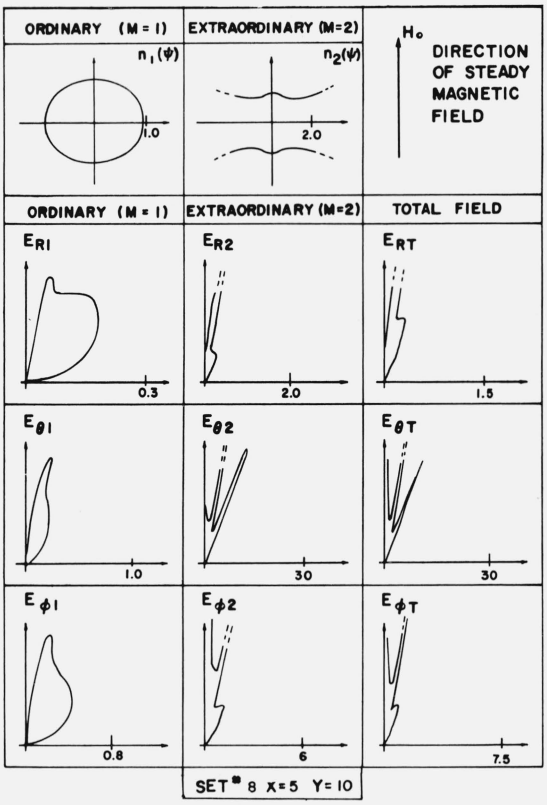

FIGURE 2. *Continued—Calculated radiation patterns for different medium parameters.*

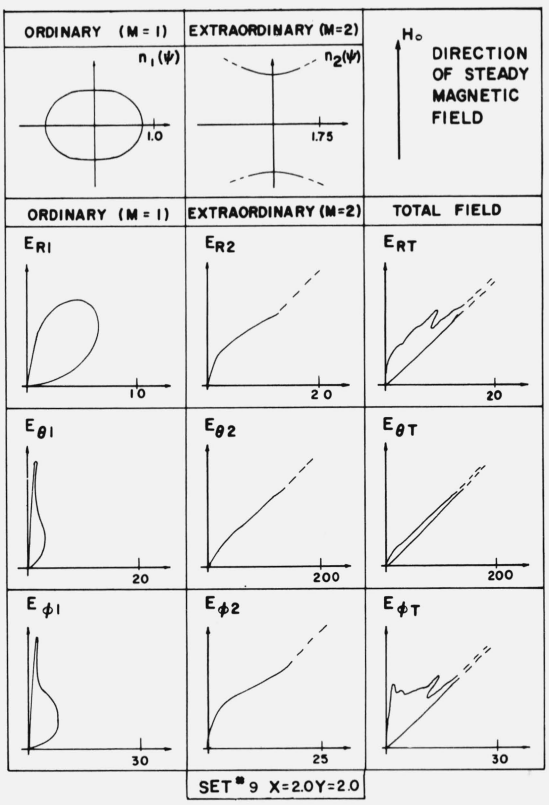

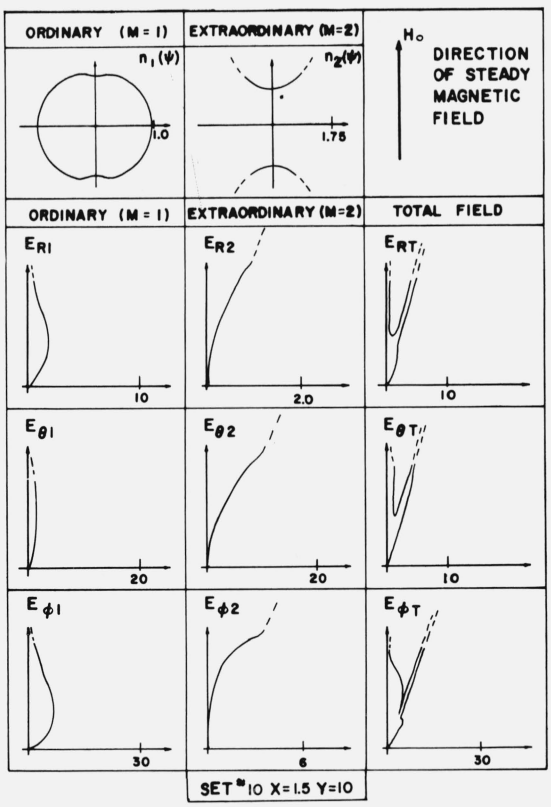

FIGURE 2. *Continued—Calculated radiation patterns for different medium parameters.*

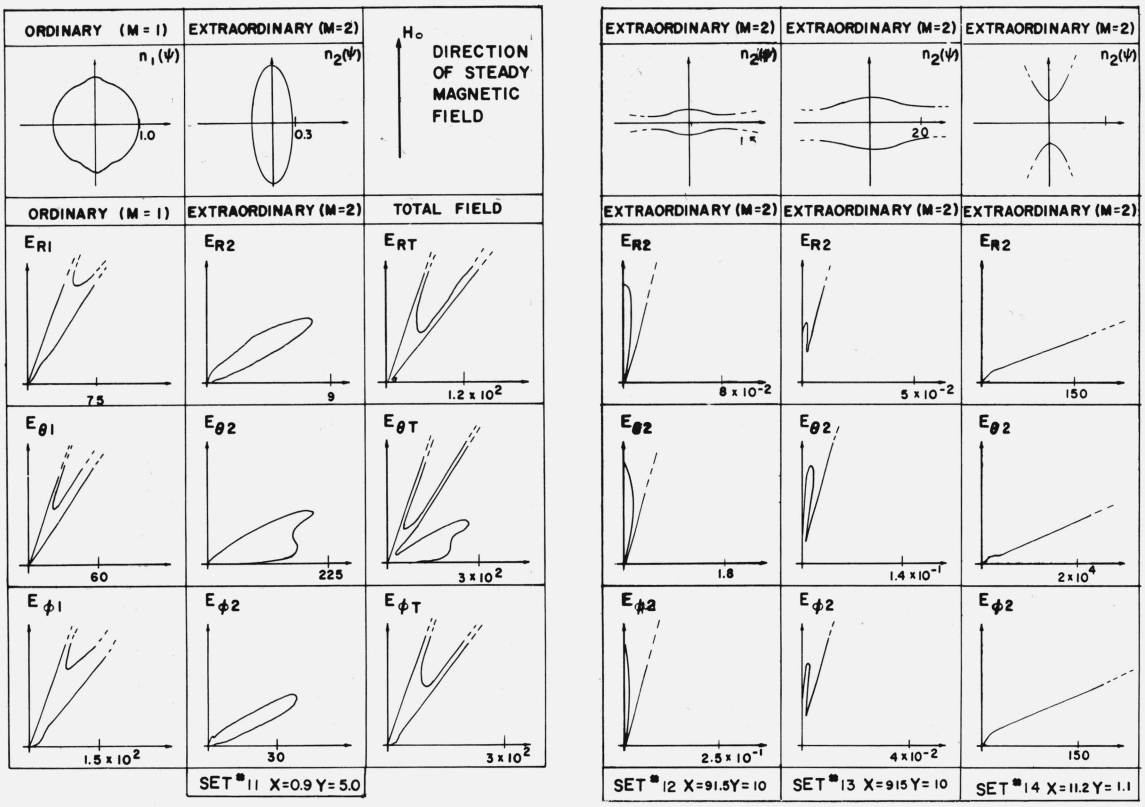

FIGURE 2. *Continued—Calculated radiation patterns for different medium parameters.*

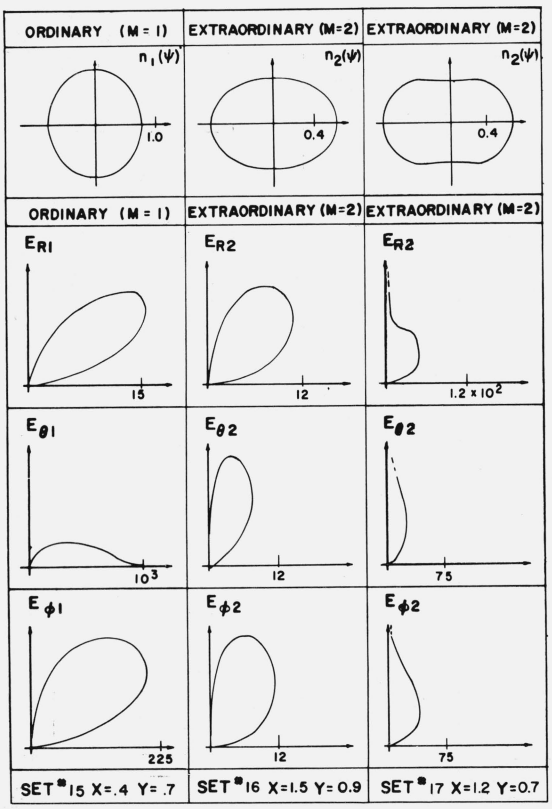

FIGURE 2. *Continued—Calculated radiation patterns for different medium parameters.*

5. Far Field Patterns

At the end of this study the far fields of a $\hat{z}$-directed dipole are given for 17 different combinations of the plasma parameters X and Y. These 17 points are shown in figure 1; corresponding calculated patterns are plotted in figure 2.

The real part of the dispersion surfaces is shown for $m=1$ and $m=2$, calculated by (22). If one or the other of the dispersion surfaces is imaginary for all θ, it is omitted completely and only the dispersion surface and the far fields for the other value of m are shown. These fields are also the total fields. Such is the case in sets numbered 12 to 17 inclusive (fig. 2). Under each dispersion curve are the corresponding ordinary or extraordinary components of the electric field, given in spherical coordinates. They are designated E_{R1}, $E_{\theta 1}$, and $E_{\phi 1}$ for the ordinary wave components and similarly for the extraordinary wave components. Broken lines indicate that this computation yields infinities. These infinities occur either when the dispersion curve contains points of inflection or when it has an open branch that goes to infinity. It should be pointed out that the double saddle point method of evaluation was not used at these points of inflection. The total far fields for $k_0 r=100$ are shown in the right hand column. All the field patterns are shown only for $0 \leq \theta \leq \pi/2$, the rest of the pattern being found through symmetry properties.

It is interesting to note the behavior of $E_{\theta T}$ at $\theta=\pi/2$ in set no. 4 (fig. 2), which is fairly close to the free space condition. This result should be compared with set no. 3 (fig. 2). Although the plasma parameters of set no. 4 (fig. 2) are still near-isotropic, the far-field pattern differs interestingly from the isotropic pattern.

The behavior of E_ϕ in set no. 11 (fig. 2) is interesting in that the ordinary and extraordinary contributions are smooth while their vector total is "modulated" quite severely. This is a direct contrast to E_θ in set no. 3 (fig. 2) and emphasizes the importance of knowing both ordinary and extraordinary components as well as the *total* fields.

As a final comment, it should be observed that the infinities which arise in this evaluation are removable. As pointed out earlier, the correct evaluation of fields at the points of inflection in terms of the Airy Integrals does yield large but finite fields. At the open branches of the dispersion curves, the infinities in the field evaluation may be removed only by assuming a finite size of dipole with a reasonably smooth current distribution. Some discussion along this line has recently appeared in an article by Staras [1964].

6. Conclusions

This study has presented Clemmow and Mulally's [1955] comprehensive classification of the dispersion curves, and figure 1 offers a useful graphical representation of this classification. Since the shapes of these curves play an important role in the calculation of the far fields, this classification permits a rough prediction of some of the pattern characteristics of the far fields of a dipole for any choice of the plasma parameters X and Y. It can also be useful in the selection of plasma parameters in practical cases where only the ordinary or extraordinary wave is desired. This may find application in the study of pattern synthesis for sources in anisotropic media.

It can be seen from (14a) that, when the refractive index curve has open branches, $\psi_{mn}=\theta$ for some θ, and A_{mn} goes to infinity. Furthermore, if a curve contains points of inflection, the Gaussian radius of curvature is zero and again field infinities will occur *in this asymptotic evaluation.* However, these infinities are removable as pointed out in the previous section. We can also note that if the refractive index curve is closed and has no points of inflection the corresponding fields will be finite for all θ. These observations are borne out by the calculations.

Another interesting observation is that the total field pattern in many cases turns out to be considerably different from the individual component patterns. It should be repeated that in general the total field pattern is dependent on the distance of the point of observation from the source because of interference between the two components. Exceptions occur when the individual patterns are highly directive and their main directions of radiation do not overlap and, of course, when one component is either absent or is largely dominated by the other.

The research reported in this study was sponsored by the National Aeronautics and Space Administration under Contract NASA NSG 395.

The authors thank S. Laxpati, who programmed the computer, and S. Kuo, who drafted the far-field patterns. Both are graduate students at the University of Illinois Antenna Laboratory.

7. References

Allis, W. P., S. J. Buchsbaum, and A. Bers (1963), Waves in anisotropic plasmas, p. 11 (MIT Press, Cambridge, Mass.).

Arbel, E. (Nov. 1960), Radiation from a point source in an anisotropic medium, Report PIB–MRI–86–60, Microwave Research Institute, Polytechnic Institute of Brooklyn.

Arbel, E., and L. B. Felsen (1963), Theory of radiation from sources in anisotropic media, Part II, Proc. Symposium on Electromagnetic Theory and Antennas (URSI) Copenhagen, 1962, p. 421–459, ed E. C. Jordan (Pergamon Press, Oxford, Eng.).

Bunkin, F. V. (1957), J. Exp. Theor. Phys. (USSR) **32,** 338–346.

Clemmow, P. C., and F. Mulally (1955), The dependence of the refractive index in magnetoionic theory on the direction of the wave normal, The Physics of the Ionosphere, 340–350 (The Physical Society, London, Eng.).

Deschamps, G. A., and O. B. Kesler (Nov. 1964), Radiation field of an arbitrary antenna in a magnetoplasma, IEEE Trans. Ant. Prop. **AP–12,** No. 6, 783.

Kogelnik, H., and H. Motz (1963), Electromagnetic radiation from sources embedded in an infinite anisotropic medium and the significance of the Poynting vector, Proc. Symposium on Electromagnetic Theory and Antennas, Copenhagen 1962, ed. E. C. Jordan, 477–493 (Pergamon Press, Oxford, Eng.).

Kuehl, H. H. (Oct. 1960), Radiation from an electric dipole in an anisotropic cold plasma, Antenna Lab. Report 24, California Institute of Technology. See also J. Phys. Fluids **5,** 1095, 1962.

Lighthill, M. J. (1960), Studies on magneto-hydrodynamic waves and other anisotropic wave motions, Phil. Trans. Roy. Soc. London **252** Ser. A, 397–430.

Mittra, R., and G. A. Deschamps (1963), Field solution for a dipole in an anisotropic medium. Proc. Symposium of Electromagnetic Theory and Antennas, Copenhagen, June 25–30, 1962, ed. E. C. Jordan (Pergamon Press, Oxford, Eng.).

Ratcliffe, J. A. (1962), The magneto-ionic theory and its applications to the ionosphere, p. 70 (Cambridge University Press, Cambridge, Eng.).

Staras, H. (Nov. 1964), The impedance of an electric dipole in a magneto-ionic medium, IEEE Trans. **AP–12,** No. 6, 695–702.

Wait, J. R. (July–Sept. 1964), Theory of radiation from sources immersed in anisotropic media, J. Res. NBS 68B, No. 3, 119–136.

(Paper 69D5–503)